ELSEVIER

Chemical Geology 200 (2003) 89–103

CHEMICAL GEOLOGY
INCLUDING
ISOTOPE GEOSCIENCE

www.elsevier.com/locate/chemgeo

Terrigenous *n*-alkane input in the South China Sea: high-resolution records and surface sediments

Carles Pelejero*

Department of Environmental Chemistry, Institute of Chemical and Environmental Research, CSIC, Jordi Girona 18, Barcelona 08034, Spain
Research School of Earth Sciences, The Australian National University, Canberra, ACT 0200, Australia

Received 2 August 2001; accepted 9 April 2003

Abstract

Molecular abundances of *n*-nonacosane are reported for a suite of 44 surface sediments and four deep sea cores distributed throughout the South China Sea (SCS), covering the last 220 ky at different time resolutions. The patterns of glacial to interglacial variability of the concentrations of this terrigenous marker are parallel for all cores, taking values linearly inversely correlated to the $U^{K'}_{37}$ index sea surface temperatures (SST), with high concentrations during cold-glacial intervals and low concentrations during warm-interglacial periods. The oscillations of this terrigenous marker likely result from the emergence and flooding of the shelves caused by sea-level variations which, together with SCS SSTs, have a clear dependency on the Northern Hemisphere climate evolution. Calculation of accumulation rates for the northernmost core together with the modern distribution of *n*-nonacosane concentrations in surface sediments evidences the complexity of sedimentation patterns in the northern SCS. In particular, and in agreement with recent studies, terrigenous materials deposited there might originate from areas different than the highly loaded Pearl River. For paleoceanographic purposes, the noticeable general pattern of the *n*-alkane concentration down-core profiles for the four cores studied, a parameter apparently unaffected by changes in sedimentation rates, prompts its use as a tracer of variations in terrigenous input into this basin over glacial to interglacial times.

Keywords: *n*-Alkanes; *n*-Nonacosane; Mass accumulation rates; South China Sea; Terrigenous input; Sedimentation rate

1. Introduction

The West Pacific marginal seas offer a unique opportunity for detailed studies of climate change over glacial to interglacial timescales since their location, between the Asian continent and the Pacific Ocean, make them very sensitive to climatic changes both on land and in the oceans (Sarnthein and Wang, 1999 and papers in the same volume). Furthermore, the high sedimentation rates of these basins allow the study of short frequency climatic oscillations. These high sedimentation rates, which can be one or two orders of magnitude higher than in the open ocean (Wang, 1999), are a consequence of the location of these marginal seas between land and open ocean, allowing them to trap most of the terrestrial sediments before they can reach the open Pacific. Another important feature of the Western Pacific Marginal seas is that they encompass the world's largest shelf areas, with water depths of 70–80 m (Gupta et al., 1987; Stattegger et al., 1997). Accordingly, the emer-

* Fax: +61-2-6125-0738.
E-mail address: carles.pelejero@anu.edu.au (C. Pelejero).

0009-2541/03/$ - see front matter © 2003 Elsevier Science B.V. All rights reserved.
doi:10.1016/S0009-2541(03)00164-5

gence of these shelf areas during glacial sea-level low stands further increased the terrigenous material supply, particularly in the South China Sea (SCS; Wang, 1999), which is the Western Pacific marginal sea that will be focused in the present study.

In the last decades, the analysis of molecular biomarkers in deep-sea sediments has become a very valuable tool for the assessment of paleoclimate changes over the Quaternary. Amongst the most studied compounds are the C_{37} alkenones, which allow the establishment of paleo-sea surface temperatures (SST) by means of the U^{K}_{37} index (initially defined by Brassell et al., 1986). This paleothermometer has gained a broad acceptance within the paleoceanographic community, as it is shown by the exponential increase in the number of publications per year based on it (Eglinton et al., 2001). These Haptophyte algae-derived organic compounds are also interpreted frequently in terms of paleo-marine primary production (e.g. Budziak et al., 2000; Villanueva et al., 2001; Schubert et al., 1998) and their $\delta^{13}C$ composition has attempted to be used to estimate paleo-pCO_2 (e.g. Andersen et al., 1999; Jasper and Hayes, 1990; Pagani et al., 1999). Other biomarkers of relevance, in terms of suitable information for paleoceanography, are long chain *n*-alkanes, which help to elucidate differences in the

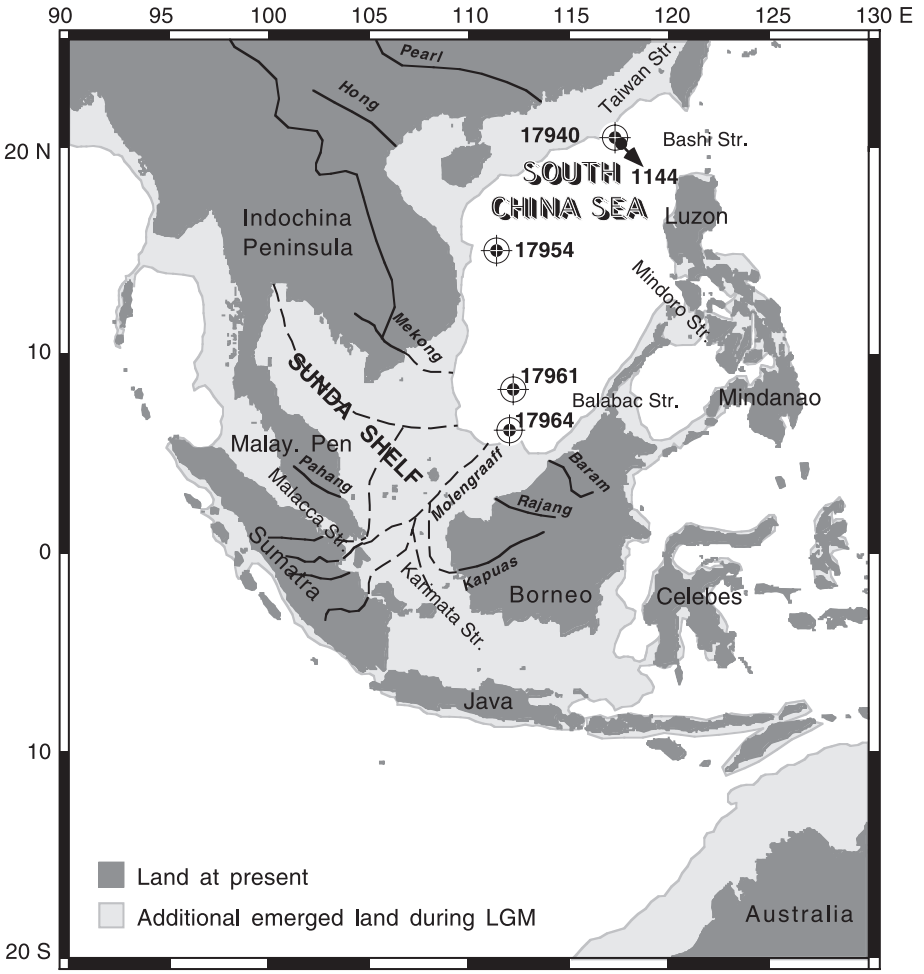

Fig. 1. Map of the South China Sea showing the location of the cores considered in this study (17940, 17954, 17961, 17954). Also depicted is ODP Site 1144, which is located only 8 km away from 17940. The approximate path of the glacial drainage systems for Moleengraaff and Palaeo-Mekong rivers according to Molengraaff (1921) and the additional emerged land during the Last Glacial Maximum are also plotted.

supply of terrigenous organic matter (e.g. Calvo et al., 2001; Ikehara et al., 2000; Ternois et al., 2001).

During the last decade, several studies based on molecular biomarkers have been performed to study the paleoceanography of the SCS. Most of these works have focused the last 30 ky, fundamentally by means of the reconstruction of temperatures (e.g. Huang et al., 1997; Kienast et al., 2001), although some of them have also attempted to integrate data on *n*-alkanes (e.g. Pelejero et al., 1999b; Steinke et al., in press). In the present work, data on abundances and fluxes of *n*-alkanes from four gravity cores spanning the last 220 ky is integrated in a comparative way to the record of $U_{37}^{K'}$ -SSTs for the same cores, which was already discussed independently in a previous study (Pelejero et al., 1999a). These comparative results are also discussed in comparison to the *n*-alkane data analysed in a suite of 44 core-tops throughout the SCS, to illustrate the modern spatial distribution of this terrigenous marker.

2. Materials and methods

2.1. Gravity cores, sedimentation rates and age models

Four gravity cores were considered in this study (17940-2, 17954-2, 17961-2 and 17964-3), which were recovered during the R/V SONNE-95 cruise in April–June 1994 (Sarnthein et al., 1994; Fig. 1 and Table 1) at roughly the same water depths (1520–1968 m; Table 1). The linear sedimentation rates of them range between 3 and 80 cm/ky depending on their location and climatic stage (see Table 1, figures and text below). As a general trend, sedimentation rates are higher during glacial than interglacial times, except core 17940 which displays the opposite trend (see further discussion below).

Table 1
Locations and water depths of the SCS gravity cores considered in this study

Core	Latitude (°N)	Longitude (°E)	Depth (m)	Sedirate (cm/ky)
17940-2	20°07.0′	117°23.0′	1727	45–80 (15–30)
17954-2	14°47.8′	111°31.5′	1520	6–7 (5–9)
17961-2	8°30.4′	112°19.9′	1968	3–8 (10)
17964-3	6°09.5′	112°12.8′	1556	~ 30 (>55)

Further details are given in Sarnthein et al. (1994) and text and figures below. Sedimentation rates in cm/ky (Sedirate) are from Wang et al. (1999a) and are presented separately for interglacial/Holocene and last glacial times (in brackets).

The age scale of all records has been adopted from Wang et al. (1999a) (see also Pelejero et al., 1999b, for more details on 17961 and 17964), which is based on AMS-^{14}C datings and on planktonic (*Globigerinoides ruber*) and benthic (*Cibicidoides wuellerstorfi*) foraminiferal δ^{18}O data. Samples were taken at 1- to 20-cm intervals depending on the sedimentation rate at the station and the period studied. The most detailed reconstruction is provided for core 17940, with a time resolution of at least bidecadal in the Holocene section. The lowest resolution is reported at sites 17961 and 17954, particularly in the oldest sections, with time intervals of ca. 5 ky per sample.

2.2. Box cores

The upper centimetres of a suite of 44 box cores throughout the SCS, recovered during the same R/V SONNE-95 cruise, were also studied (Table 2). According to current sedimentation rates, this upper centimetre should correspond roughly to the last 20 to 200 years, depending on each location.

2.3. Analytical methods

The procedures and equipment used for $U_{37}^{K'}$ index and long chain *n*-alkane determinations are described elsewhere (Villanueva et al., 1997). Briefly, sediment samples were freeze-dried and manually ground for homogeneity. After addition of an internal standard (a mixture of *n*-nonadecan-1-ol, *n*-hexatriacontane and *n*-tetracontane), subsamples (ca. 3 g) were extracted with dichloromethane in an ultrasonic bath. The extracts were hydrolyzed with 6% potassium hydroxide in methanol to eliminate interferences from wax esters. After bis(trimethylsilyl)trifluoroacetamide derivatization, the extracts were analyzed by gas chromatography (GC) equipped with a flame ionization detector in order to quantify long-chain ketones and long-chain *n*-alkanes.

With this simple clean-up and quantification method, neither alkenones nor *n*-nonacosane was presenting coeluates. However, in order to properly isolate

Table 2
Locations and water depths of the box cores from which *n*-nonacosane concentrations in surface sediments were determined

Core	Latitude (°N)	Longitude (°E)	Depth (m)	*n*-Nonacosane (ng/g)
17920-1	14°35.1′	119°45.1′	2507	24
17921-1	14°54.7′	119°32.3′	2507	53
17922-1	15°25.0′	117°27.5′	4221	15
17924-1	19°24.7′	118°50.8′	3438	172
17925-2	19°51.1′	119°02.8′	2980	132
17926-2	19°00.0′	118°44.0′	3761	163
17928-2	18°16.3′	119°44.7′	2486	65
17929-1	20°40.9′	115°42.0′	371	34
17930-1	20°20.0′	115°46.9′	629	70
17931-1	20°06.0′	115°57.8′	1005	70
17932-1	19°57.0′	116°02.3′	1365	35
17933-2	19°32.0′	116°13.6′	1972	145
17934-1	19°01.9′	116°27.7′	2665	141
17935-2	18°52.7′	116°31.6′	3143	129
17936-1	18°46.0′	117°07.2′	3809	106
17937-1	19°30.1′	117°40.0′	3428	157
17938-1	19°47.2′	117°32.3′	2835	169
17939-1	19°58.2′	117°27.3′	2473	174
17940-1	20°07.0′	117°23.0′	1728	248
17941-1	21°30.9′	118°28.9′	2201	129
17942-1	19°20.0′	113°12.1′	329	37
17943-1	18°57.0′	113°33.2′	917	104
17944-1	18°39.3′	113°38.2′	1219	75
17945-1	18°07.6′	113°46.6′	2404	128
17946-1	18°07.5′	114°15.0′	3465	118
17947-2	18°28.0′	116°01.7′	3765	131
17948-1	18°42.5′	114°53.8′	2841	66
17949-1	17°20.9′	115°10.0′	2195	72
17950-1	16°05.6′	112°53.9′	1868	153
17951-1	16°17.3′	113°24.6′	2340	61
17952-2	16°40.0′	114°28.4′	2882	69
17953-3	14°33.0′	115°08.6′	4307	92
17954-1	14°45.5′	111°31.6′	1517	91
17955-1	14°07.3′	112°10.6′	2404	72
17956-1	13°50.9′	112°35.3′	3387	63
17957-1	10°53.9′	115°18.3′	2197	35
17958-1	11°37.3′	115°04.9′	2581	62
17959-1	11°08.3′	115°17.2′	1957	39
17960-1	10°07.1′	115°33.3′	1707	62
17961-1	8°30.4′	112°19.9′	1795	99
17962-1	7°10.9′	112°04.9′	1970	83
17963-2	6°10.0′	112°40.0′	1233	100
17964-1	6°09.5′	112°12.8′	1556	98
17965-1	6°09.4′	112°33.1′	889	55

These cores were retrieved during the SONNE-95 cruise (Sarnthein et al., 1994).

and detect the complete set of terrestrially derived long-chain alkanes (namely C_{25} to C_{33} *n*-alkanes), a further clean-up step based on silica gel column chromatography was performed on selected samples of core 17961 (see Section 3.1) after the potassium hydroxide hydrolysis.

Compound quantification is based on the internal standard peaks, involving correction for internal standard recovery which was always better than 90% (the response factor of the biomarkers relative to the standards was assumed to be 1). Six times replication of sediment samples with similar lipid content showed standard deviations of 8% in *n*-alkane concentration estimations. For the computation of fluxes, the original concentrations were multiplied by the sedimentation rate and the dry bulk density (Wang, unpublished data).

Concerning the SST measurements, which were estimated using the SCS equation $U^{K'}_{37} = 0.031\mathrm{SST} + 0.092$ (Pelejero and Grimalt, 1997), six times replication of sediment samples with similar lipid content and $U^{K'}_{37}$ index showed standard deviations of ± 0.15 °C.

3. Results and discussion

3.1. n-Alkanes composition

The *n*-alkane mixture of the sediments from the SCS is rather uniform, with the distributions of homologous compounds ranging between C_{23} and C_{33}, maximizing at C_{31} and with an odd to even carbon number preference evidencing a typical higher-plant origin (Peltzer and Gagosian, 1989). This can be observed in Fig. 2, which presents data on the Carbon Preference Index (CPI) and Average Chain Length (ACL) for a suite of samples from the southern core 17961, for which a further than normal clean-up step allowed the analysis of the whole terrigenous *n*-alkane series (C_{23} to C_{33}; see Section 2.3).

CPI values in this particular location oscillate between 2.3 and 4.6, matching precisely CPIs observed in deep-sea sediments from the western tropical Pacific Ocean (2.6–4.0; Ohkouchi et al., 1997b). SCS Holocene CPIs of about 2.3 (Fig. 2) also agree with data obtained from surface sediments from the open tropical Pacific Ocean at the same latitudes (Ohkouchi et al., 1997a), although the eolian trade wind transport mechanism for *n*-alkanes suggested there might not be the same for the SCS. In fact, the modern eolian

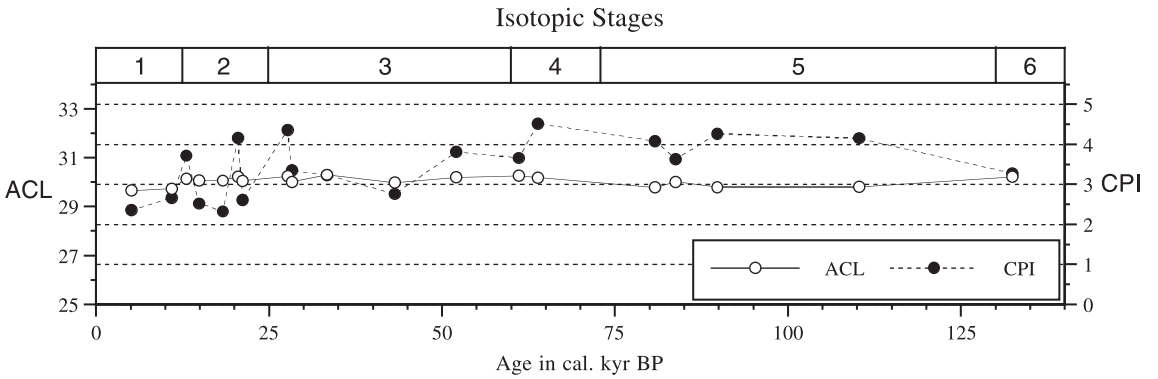

Fig. 2. CPI ($CPI = 4 \times [[C_{25}]+[C_{27}]+[C_{29}]+[C_{31}]+[C_{33}]]/5 \times [[C_{26}]+[C_{28}]+[C_{30}]+[C_{32}]]$) and ACL ($ACL=[\Sigma[C_i] \times i]/\Sigma[C_i]$ for $i=25$ to 33) indexes for a suite of samples from southern core 17961. C_i is the concentration of the *n*-alkane containing *i* carbon atoms.

contribution to deep-water sediments from Western Pacific marginal seas is negligible (Wang, 1999), and a fundamentally fluvial transport can be accounted for most of the modern SCS basin, with the only exception of the northernmost areas (Wang et al., 1999a).

The ACL values suggest homogeneous average *n*-alkane chain lengths throughout the last 140 ky, with values between 29.7 and 30.3 (Fig. 2). This constant *n*-alkane length suggests that potential variations due to ecological and/or environmental change do not affect the glacial/interglacial record of terrigenous organic matter.

The analysis of the complete set of long-chain *n*-alkanes in this suite of 17961 samples displayed a highly significant linear correlation ($R=0.974$; not shown) between *n*-nonacosane abundances and total odd carbon numbered long-chain *n*-alkanes (C_{25}, C_{27}, C_{29}, C_{31} and C_{33}), with *n*-alkanes concentration being always about four times the value of *n*-nonacosane concentration. This observation justifies the simplified use of only *n*-nonacosane to monitor the complete set of long-chain *n*-alkanes in the SCS sedimentary records, as it is done in the following.

3.2. n-Nonacosane concentrations as compared to SSTs

When compared to the glacial to interglacial evolution of SSTs, *n*-nonacosane abundances depict a clear and very robust inverse relationship with maximum concentrations during glacial periods and minimum values during interglacials (Fig. 3). Linear curve fitting of these two proxies result in a significant inverse linear correspondence for the four cores, with correlation coefficients (R) between 0.82 and 0.87 (Table 3). All concentration profiles of *n*-nonacosane display a comparable glacial to interglacial pattern with the only difference that the coastal cores (17940 and 17964) reach to substantially higher values during glacial periods (500–550 vs. 150–200 ng/g) than the open sea cores (17961 and 17954). This observation is consistent with a more important terrigenous influence for sites closer to the coast during low sea-level times.

The simultaneous recording of such inverse pattern of alkanes vs. SSTs at four sites distributed amongst different SCS areas suggests that this might be a general characteristic for the whole SCS (although further studies would help corroborate this assertion). This inverse pattern can be explained by the close link that exists between sea level and terrigenous inputs as well as global SSTs: During glacial sea-level low stands, the emergence of the huge continental platforms in the north and south of the SCS led to the development of numerous drainage systems (like the so-called Molengraaff river over Sunda Shelf; Molengraaff, 1921) that significantly increased the input of terrestrial material and thus *n*-alkanes into this marginal sea (e.g. Schönfeld and Kudrass, 1993). In contrast, during and after the inundation of the shelf areas, the retreat of the coastline, together with the disappearance of the important drainage systems led to a drastic drop in the supply of terrestrial organic matter (Figs. 1 and 3).

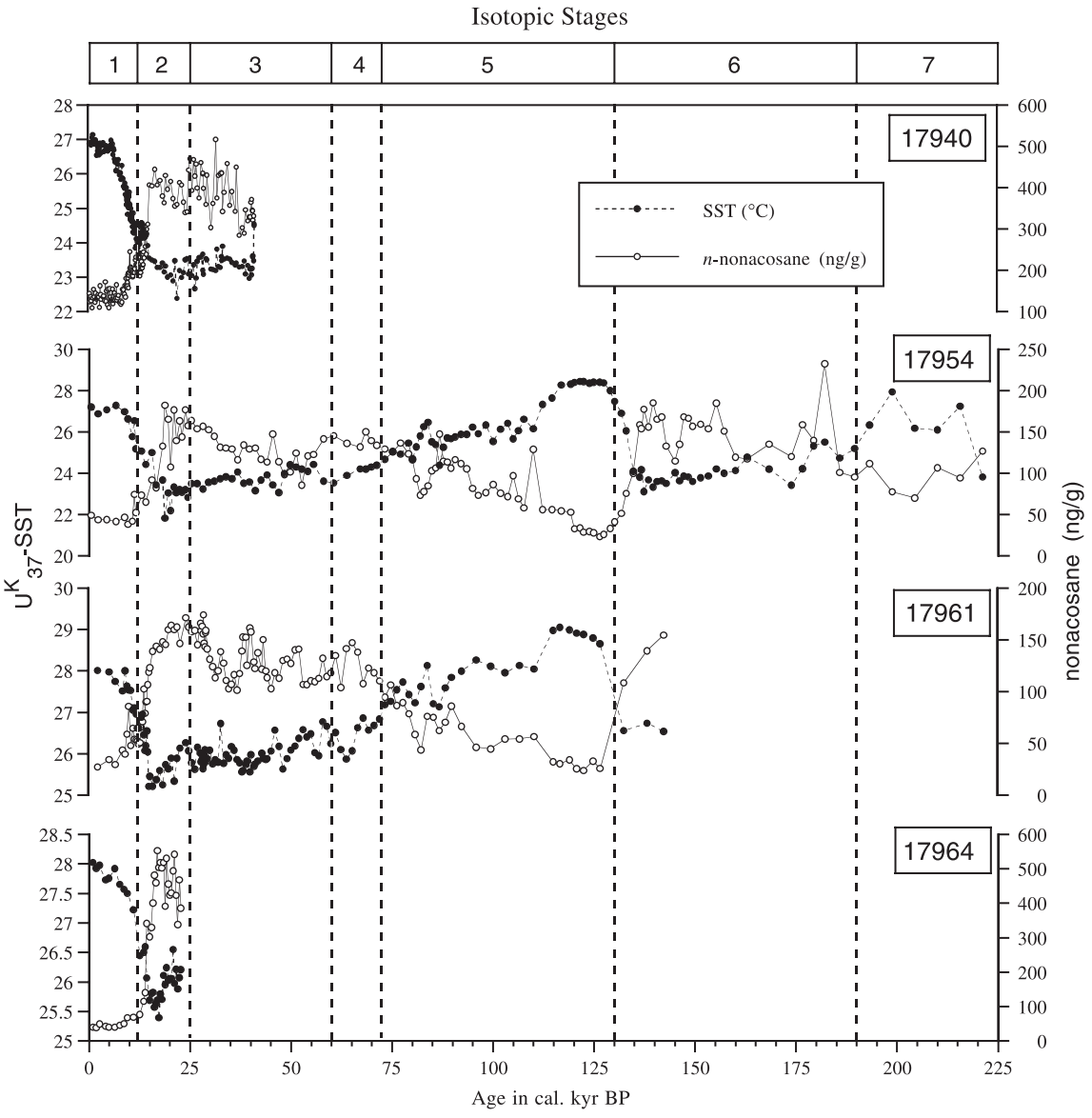

Fig. 3. *n*-Nonacosane abundances (solid line and open circles) and U^K_{37}-SSTs (dashed line and filled circles) for the four SCS cores studied. SSTs were estimated using the SCS equation $U^K_{37} = 0.031SST + 0.092$ (Pelejero and Grimalt, 1997), representing annual average temperatures at the 0–30-m depth.

Concerning SSTs, the values encountered in the SCS have been shown to follow precisely the Northern Hemisphere temperature evolution, particularly during the last deglaciation, when the major SCS SST increase has been shown to occur synchronously with the Bølling warming in the Greenland GISP2 ice-core record (Kienast et al., 2001). Additionally, the concurrence of this deglacial SST increase with an abrupt decrease of *n*-alkanes has recently been linked to Melt Water Pulse (MWP) Ia, an observation which implies a synchroneity between this event and the Bølling warming (Kienast et al., 2003). As it is discussed in the latter study, a direct linking mechanism of drastic warming events causing the rapid

Table 3
Linear correlations between SST and *n*-nonacosane concentrations (C_{29})

CORE	*n*	SST vs. C_{29} (ng/g)
17940	183	$C_{29} = -70 \times SST + 1976$ $R = 0.862$ $R^2 = 0.742$
17954	128	$C_{29} = -22 \times SST + 671$ $R = 0.822$ $R^2 = 0.676$
17961	126	$C_{29} = -37 \times SST + 1090$ $R = 0.845$ $R^2 = 0.714$
17964	35	$C_{29} = -203 \times SST + 5704$ $R = 0.871$ $R^2 = 0.759$

n = number of data points.

melting of ice sheets could be suggested as one possible explanation for such synchronic responses (within the resolution of deep sea sediments) on both the evolution of temperatures and the terrigenous *n*-alkanes input into the SCS.

A part from last deglaciation, the same or a similar forcing mechanism affecting both temperature and terrigenous input seems to have operated in the SCS during, at least, the last 220 ky. Such continuous forcing, very likely via sea-level oscillations and ice volume, is suggested after the observation that the inverse relationship of *n*-nonacosane concentrations with SSTs is maintained in all the four cores studied for the whole covered period. Moreover, this inverse pattern also includes specific events such as the brief warming excursion centred at about 85 ka BP, recorded at sites 17954 and 17961 as a *n*-nonacosane minima.

3.3. n-Nonacosane fluxes vs. concentrations

It is often useful to calculate fluxes (or mass accumulation rates) in order to avoid problems associated with dilution of the biomarker abundances. Such values for *n*-nonacosane have been computed and represented in Fig. 4, together with *n*-nonacosane concentrations, sedimentation rates and U^K_{37}-SSTs, for comparison.

The age profiles of the *n*-nonacosane fluxes for cores 17954, 17961 and 17954 appear to maintain a similar inverse relationship with temperature, in the same way than *n*-nonacosane concentrations. However, this correlation is not followed in core 17940, where values of *n*-nonacosane fluxes for the glacial period are not consistently higher than during the Holocene. This difference is a direct result of the singular sedimentation rates exhibited at core 17940, which are substantially higher during the Holocene than during the glacial, a counterintuitive pattern opposite to what is encountered for the rest of the cores.

The fact that the glacial to interglacial profiles of *n*-nonacosane concentrations for all four cores studied are parallel, a result also revealed by *n*-nonacosane fluxes from cores 17954, 17961 and 17964, suggests that the singular differences in *n*-nonacosane fluxes for core 17940 might be a result of either inaccuracies in the age model (and thus sedimentation rate) or altered sedimentation processes.

The age model of this core was initially constructed based on 40 AMS-^{14}C ages, applying a smooth spline to eliminate unrealistic strongly fluctuating sedimentation rates (Wang et al., 1999a). However, serious unknowns in the conversion of ^{14}C ages into calendar ages (particularly for sections older than 11,600 years BP) prompted the construction of an alternative age model (Wang et al., 1999a) based on comparison of the planktonic foraminifera δ^{18}O record with the δ^{18}O curve of the GISP2 ice core (Grootes and Stuiver, 1997). This latter age model, which assumes that foraminifera δ^{18}O reflects periods of maximum monsoon precipitation closely linked to warm episodes in Greenland, has been adopted in several paleoceanographic reconstructions based on this core (e.g. Pelejero et al., 1999a; Wang and Sarnthein, 1999) and has formed the basis of the chronostratigraphy of a newer neighbouring core, ODP Site 1144, located only 8 km southeast from 17940 (Fig. 1; Bühring et al., in press).

In Fig. 4, fluxes of *n*-nonacosane for core 17940 have been calculated with both independent age models, resulting in significant differences for sections older than 11.6 ky BP, when both age models diverge. In particular, *n*-nonacosane fluxes with the original model using the AMS-^{14}C dates exhibit nearly homogeneous values of about 7 μg/cm^2 ky, while using the age model tied to Greenland, *n*-nonacosane fluxes display three well-defined excursions reaching to 10–20 μg/cm^2 ky, superimposed to a

roughly constant base line of about 4–5 μg/cm^2 ky. These differences are a direct consequence of the dissimilarities that exist between both sedimentation rates depending on each age model (although none of the age models suggested is capable of reproducing the clear glacial high and Holocene low pattern of *n*-nonacosane concentrations).

This contrasting results can be taken as an example on how dependent is the computation of fluxes on sedimentation rate values, which strongly depend, in

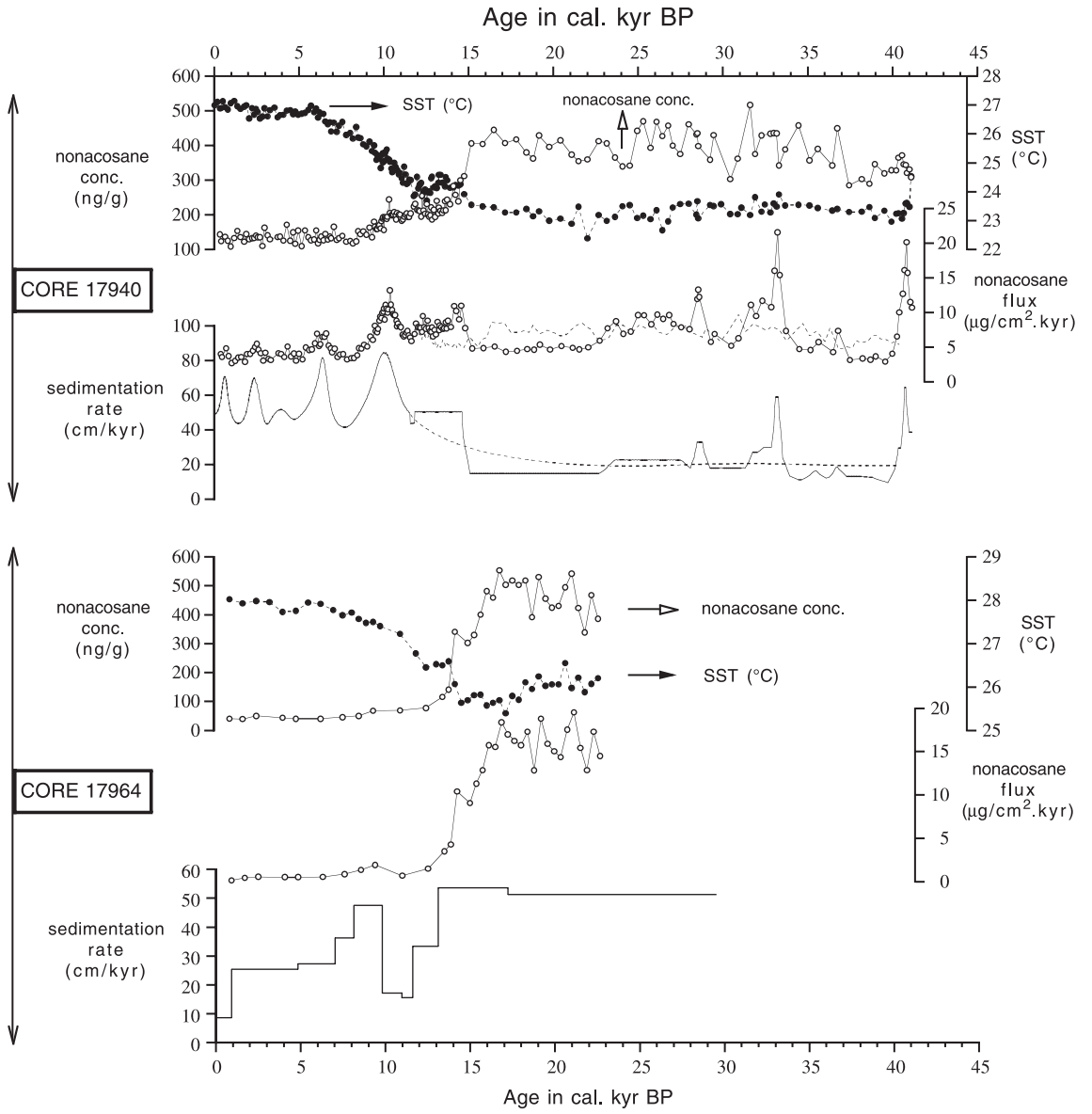

Fig. 4. Sedimentation rates, *n*-nonacosane fluxes and concentrations and SSTs for cores 17940 and 17964, which are the most proximal to the coast and for cores 17954 and 17961, which are located further offshore. In the case of core 17940, two alternative age models were used to estimate sedimentation rates and fluxes, after Wang et al. (1999a) (see text). Note the apparent decoupling between *n*-nonacosane fluxes and concentrations for core 17940, independent of the age model chosen.

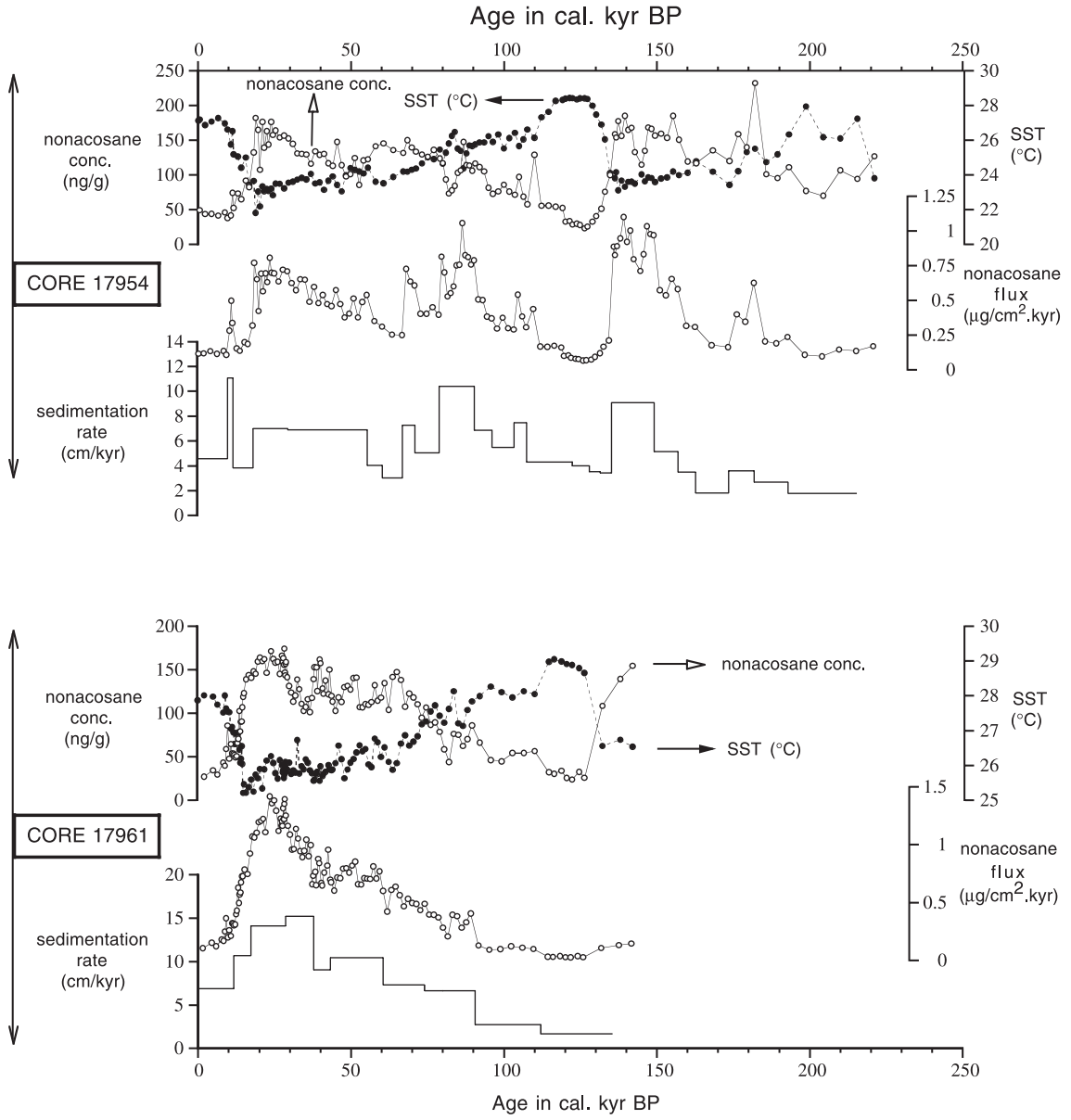

Fig. 4 (*continued*).

their turn, on the quality of the age model. In fact, the dependency of fluxes versus sedimentation rates is well illustrated in the work by Middleburg et al. (1997), where the authors report a spurious correlation (with $R^2 = 0.98$) between a randomly generated carbon burial rate and sedimentation rates. Thus, for settings where sedimentation rates display important changes in time, any computed flux profile will tend to resemble the sedimentation rate curve.

As already mentioned, there are still many unknowns to accurately convert ^{14}C ages in this area to calendar ages during last deglaciation and Marine Isotope Stage 3, including uncertainties in the local reservoir age. In this sense, a recent study on the same

core has suggested that reservoir ages during last deglaciation might have increased as much as 1200–1300 years at this site, possibly due to advection of Pacific Intermediate waters (Kienast et al., 2003). Uncertainties in this parameter as well as the need to better constrain the cosmogenic paleo-^{14}C production thus prevents the establishment of an unequivocal age model for core 17940.

Considering again the recently studied neighbouring core ODP 1144, which is located at only 8 km from 17940, it is worth to remark that sedimentation rates there have been shown to display the normal pattern exhibited in cores from the SCS, with higher values during glacial times (particularly Stage 2) than during the Holocene (Bühring et al., in press; Higginson et al., in press). These sedimentary differences are even more surprising since the age model for ODP 1144 was constructed by correlation to the $\delta^{18}O$ record of GISP2, by analogy to the most used age model of 17940, as it has already been mentioned.

Thus, if this latter chronostratigraphic option is assumed to be correct, there should be an explanation on why this drastic glacial changes in *n*-nonacosane fluxes at core 17940 were not effectively translated into similar variations in the sedimentary concentration of *n*-nonacosane, and why two cores only 8 km apart displayed such a different pattern of sedimentation.

3.4. Anomalous sedimentation patterns in the northern SCS

The specific reasons for these counterintuitive glacial to interglacial sedimentation rates in core 17940 are unknown. However, some suggestions can be listed to account for this pattern.

Winnowing could be ascribed as one possibility, since this process is likely to have occurred at 17940 core location, particularly during glacial times, as reported by Wang et al. (1999a,b). In these studies, evidences of glacial winnowing were obtained from data on particle sizes, which were studied in terms of the 'Koopman index' (Koopmann, 1981). Using this index, which allows for a qualitatively estimation of winnowing effects, signs of alternation between winnowed and unwinnowed samples were reported in core 17940, especially for the glacial sections, which is the period displaying anomalous low sedimentation rates. One possibility is that glacial winnowing and thus, removing of deposited material, might have artificially lowered sedimentation rates during this period. In this case, and after a homogeneous removal of the deposited sediments (which might not necessarily be the case) the *n*-alkane concentrations of the non-winnowed material could have remained intact, preserving the original glacial higher terrigenous signature, while fluxes would display artificially lowered values. However, some complex transport mechanism or morphological feature (ca. bottom relief) should also be taken into account to explain winnowing at 17940 location but not at ODP 1144, given that the latter displays the "usual" high glacial sedimentation rates.

A deviation during glacial times of the large sediment load from Pearl River due to changes of main river flow direction when sea level was low is another possibility (Wang et al., 1999a). This scenario would explain why during glacial times, other gravity cores taken in the vicinity of 17940, but further offshore, displayed higher sedimentation rates than this one (Wang et al., 1999a). As these authors conjecture, perhaps the sediment load bypassed the location of core 17940, due to river mouth shifts across the shelf induced by sea-level lowering. However, this circumstance would hardly explain why during these glacial periods of low sedimentation, *n*-alkane concentrations displayed such consistently high values. In fact, interpretations from new seismic profiles for this area argued against any glacial sediment load bypass and suggested an alternative explanation (Lüdmann et al., 2001). These authors ascribed differences in sedimentation rates to the relative exposure of Dongsha Islands, which are located upslope to the northwest of cores 17940 and 1144. During glacial times, the higher elevation of these islands could have deviated the sediment supply to the more basin-ward located coring station.

However, sedimentation mechanisms at this particular area of the northern SCS might be even more sophisticated, and provenances of terrigenous material different than the Pearl River have been suggested in several occasions. Some years ago, an attribution of sediments transported from the East China Sea and the Pacific via the Bashi Strait was suggested (Wang, 1999) based on data from sediment traps (Jennerjahn et al., 1992). More recently, a geochemical study on

samples from the neighbouring core ODP 1144, has evidenced that sediments in this particular location do not originate from the Pearl River (Shao et al., 2001). On the contrary, the triangular La–Th–Sc and Th–Sc–Zr/10 diagrams presented by these authors suggest that sediments might more likely derive from Taiwan, an origin which has probably remained constant during the last million years. In fact, and as compiled by Milliman and Meade (1983) the annual sediment discharge carried to the oceans from torrential Taiwanese Rivers is spectacular. For instance, and according to this data, Choshui River, which debouches to the west of the island to Taiwan Strait, accounts for almost as much annual sediment delivery (66 millions of tonnes per year) as the Pearl River (69 millions of tonnes per year). The present contribution of terrigenous material from Taiwan to northern SCS deep-sea sediments is also in agreement with data on pollen and *n*-alkanes from surface sediments, as it is described in the following section.

3.5. Modern surface distribution of terrigenous n-alkanes

Further insight into the peculiarity of sedimentation into the SCS can be obtained from the determination of *n*-nonacosane abundances from surface sediments. With this aim, a total of 44 surface sediments throughout the SCS were analysed, displaying *n*-nonacosane concentrations in the 15–250 ng/g range (Fig. 5; Table 2). Surprisingly, the higher values are not encountered closer to the river mouths, as it would have been expected. On the contrary, maximum values of about 160 to 250 ng/g are confined to the northeastern area (cores 17937–17940), as the krigging interpolated surface data shown in Fig. 5 clearly evidences. In fact, this area with maximum concentrations of *n*-nonacosane includes core 17940, which is the core discussed above with counterintuitive sedimentation rates and, perhaps, anomalous sedimentation patterns.

This surface data on *n*-nonacosane concentration is in good agreement with data on pollen studied from approximately the same suite of core-tops (Sun et al., 1999). For instance, the concentration of pollen and spores was found maximum also in the northeastern SCS, adjacent to the Taiwan and Bashi Straits, exactly where *n*-nonacosane concentrations are highest. Moreover, pollen and spores from samples towards the Pearl River displayed substantially lower abundances by as much as 1.5 order of magnitude. As suggested by Sun et al. (1999) and in agreement with sediment trap data from Jennerjahn et al. (1992), this pollen pattern could be explained by an oceanic or eolian provenance from Bashi and Taiwan Straits during winter monsoon periods (November–January), when sedimentary influx from this areas is maximum. A similar origin could then also be ascribed to the modern distribution of *n*-alkanes in the northern SCS, which would be also in agreement with the latest geochemical results from Shao et al. (2001) already discussed.

Hydrodynamic sorting of lipids between different grain sizes could also explain, in part, why *n*-alkanes are more abundant further offshore from Pearl River mouth than closer to the coast. It has long been recognised that the finest particles are usually enriched in organic matter and/or hydrocarbons compared to coarser grains (e.g., Bordovskiy, 1965; Thompson and Eglinton, 1978). Since such fine particles are more easily transported to longer distances than coarse materials, an enrichment of terrigenous organic markers further offshore could take place.

In the southern SCS, *n*-nonacosane abundances for box cores 17961–17965 display rather homogeneous values of about 90 ng/g, which are substantially lower than the northern SCS maximum discussed above (Fig. 5). These results are again in agreement with pollen analyses in the southern SCS, where lower abundances were also reported (Sun et al., 1999). Moreover, the clear inshore lowering tendency in *n*-nonacosane concentrations exhibited towards Pearl River is not displayed in the southern SCS, indicating a more direct origin of this terrigenous matter from either Borneo or Vietnam. Similarly than Taiwan, the highly erosive mountainous rivers from Borneo deliver huge amounts of sediment to the SCS, with sediment yields of up to 459 millions of tonnes per year, as compiled by Milliman et al. (1999). This north to south apparent difference in provenance of terrigenous materials further corroborates the singularity of the northern SCS area, where core 17940 is located, in terms of sedimentation.

Sedimentation patterns in this SCS area are thus still obscure at the moment, and further research on

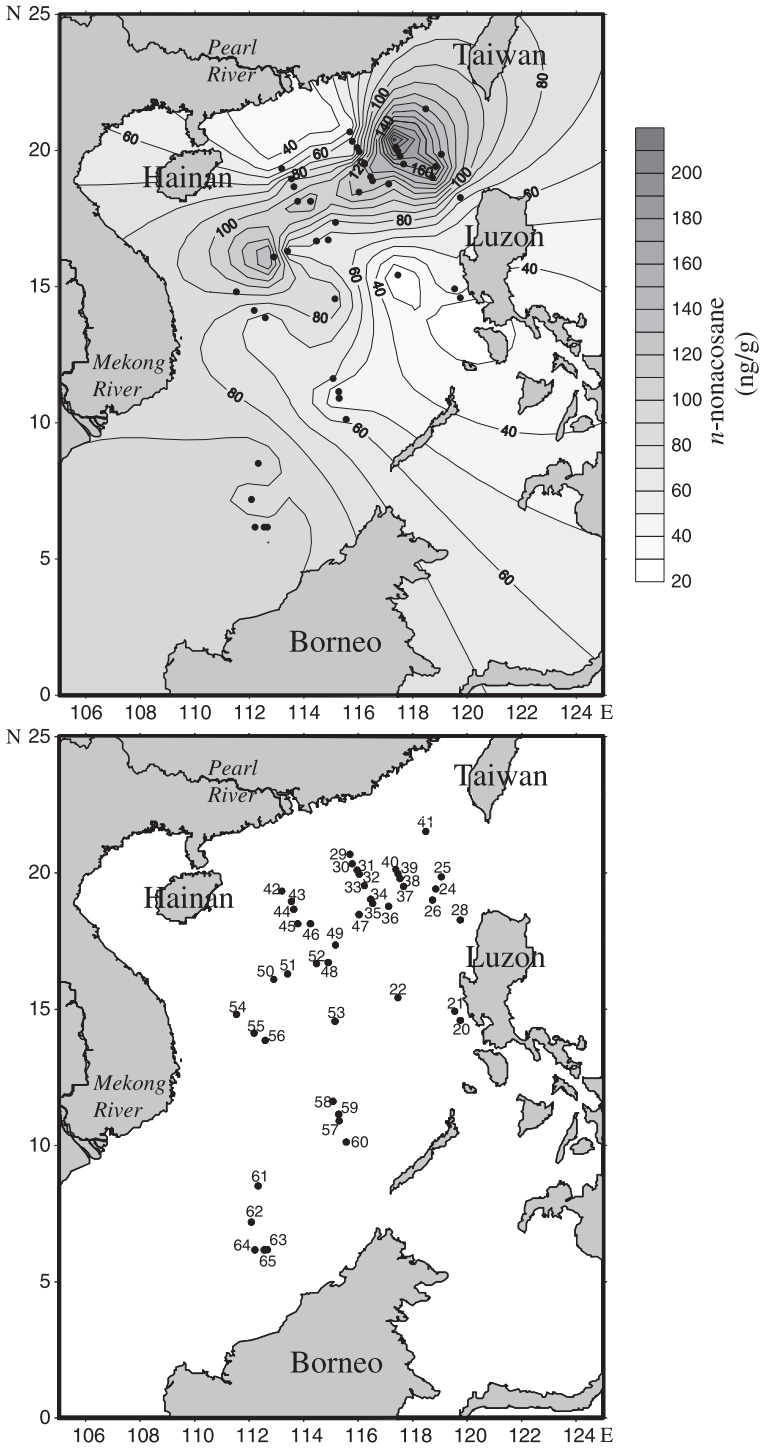

Fig. 5. *n*-Nonacosane abundances from surface sediments after interpolation of raw data (Table 2) with the krigging method (upper panel). Location of all studied surface sediments (lower panel; box core numbers omit the first three digits which were 179 in all cases, see Table 2 for exact location).

provenance of deposited materials and transport mechanisms is needed. Meanwhile, and for paleoceanographic purposes, the noticeable general pattern of the *n*-alkane concentration down-core profiles for the four cores studied, a parameter apparently unaffected by changes in sedimentation rates, prompts its use as a tracer of variations in terrigenous input into this basin over glacial to interglacial times.

4. Conclusions

A detailed analysis of the complete set of long-chain *n*-alkanes in one core from the central southern SCS shows carbon preference index values of 2.3 to 4.6 and average chain lengths of 29.7 to 30.3 throughout the last climatic cycle, suggesting limited changes in the composition of organic matter delivered to the South China Sea on a glacial–interglacial timescale. A significant correlation exists between total terrestrial *n*-alkanes and only *n*-nonacosane, which justifies the simplified use of only *n*-nonacosane to monitor the complete set of long-chain *n*-alkanes in the SCS sedimentary records.

Concentrations of the terrestrial marker *n*-nonacosane studied in four SCS cores spanning the last 220 ky BP display a clear glacial to interglacial pattern with higher values during glacial stages and low concentrations during interglacials, a pattern which depicts a robust inverse relationship to SSTs. The oscillations of this terrigenous marker likely result from the emergence and flooding of the shelves caused by sea-level variations which, together with SCS SSTs, have a clear dependency on the Northern Hemisphere climate evolution.

When *n*-nonacosane concentrations are computed into fluxes, all cores appear to maintain a similar inverse relationship with temperature, in exception of core 17940, where values of *n*-nonacosane fluxes for the glacial period are not consistently higher than during the Holocene. This difference is a direct result of the singular sedimentation rates exhibited at core 17940, which are substantially higher during the Holocene than during the glacial, a counterintuitive pattern opposite to what is encountered for the rest of the cores. The fact that core ODP 1144, taken only 8 km away from 17940, presents the SCS typical high glacial/low Holocene sedimentation rate pattern evidences the complexity of the northern SCS in terms of sedimentation.

These results from 17940 can be taken as an example on how dependent is the computation of fluxes on sedimentation rate values, which strongly depend, in their turn, on the quality of the age model. For this reason, we recommend to include always the original concentration values and/or the estimated sedimentation rates in the studies where accumulation rates are decided to be reported.

The modern abundances of *n*-nonacosane in the SCS sediments display highest concentrations in the northeastern area, where core 17940 is located. This pattern parallels the reported modern distribution of pollen and spores in surface sediments, suggesting a possible eolian or oceanic origin of these terrigenous materials from Taiwan and Bashi Straits. This idea is also in agreement with recent geochemical data from core ODP 1144, which evidences that other areas different than Pearl River might play a more important role in delivering terrigenous matter to the northern SCS.

Further research on provenance of deposited materials and transport mechanisms is needed to fully understand the sedimentation of the northern SCS. For paleoceanographic purposes, the noticeable general pattern of the *n*-alkane concentration down-core profiles for the four cores studied, a parameter apparently unaffected by changes in sedimentation rates, prompts its use as a tracer of variations in terrigenous input into this basin over glacial to interglacial times.

Acknowledgements

I thank E. Calvo, S. Kienast, and M. Kienast for constructive discussions and my late friend Luejiang Wang for providing the dry bulk density data and for transmitting me his devotion to paleoceanography. J. Grimalt is also acknowledged for analytical facilities at Department of Environmental Chemistry (ICER-CSIC), Barcelona. I am very grateful to Malcolm McCulloch and Graham Logan for providing the opportunity and facilities to work at RSES and Geoscience Australia, Canberra, respectively. This work was supported by a PhD grant from C.I.R.I.T. (Generalitat de Catalunya) during the experimental work and by Spanish Secretaria de Estado de

Educación y Universidades during the writing of this manuscript. The samples included in this study were collected during a R/V SONNE cruise, funded by the German Ministry for Education and Research (BMBF). **[LW]**

References

Andersen, N., Müller, P.J., Kirst, G., Schneider, R.R., 1999. Alkenone $\delta^{13}C$ as a proxy for past pCO_2 in surface waters: results from the Late Quaternary Angola current. In: Fischer, G., Wefer, G. (Eds.), Proxies in Paleoceanography: Examples from the South Atlantic. Springer, Berlin, pp. 469–488.

Bordovskiy, O.K., 1965. Accumulation and transformation of organic substances in marine sediments: 3. Accumulation of organic matter in bottom sediments. Mar. Geol. 3 (1–2), 33–82.

Brassell, S.C., Eglinton, G., Marlowe, I.T., Pflaumann, U., Sarnthein, M., 1986. Molecular stratigraphy: a new tool for climatic assessment. Nature 320, 129–133.

Budziak, D., et al., 2000. Late Quaternary insolation forcing on total organic carbon and C_{37} alkenone variations in the Arabian Sea. Paleoceanography 15 (3), 307–321.

Bühring, C., Sarnthein, M., Erlenkeuser, H., in press. Toward a high-resolution stable isotope stratigraphy of the last 1.1 million years: Site 1144, South China Sea. Proceedings of the Ocean Drilling Program, scientific results. Texas A&M University Ocean Drilling Program, College Station, TX, United States, vol. 184.

Calvo, E., Villanueva, J., Grimalt, J.O., Boelaert, A., Labeyrie, L., 2001. New insights into the glacial latitudinal temperature gradients in the North Atlantic. Results from $U^{K'}_{37}$-sea surface temperatures and terrigenous inputs. Earth Planet. Sci. Lett. 188, 509–519.

Eglinton, T.I., Conte, M.H., Eglinton, G., Hayes, J.M., 2001. Proceedings of a workshop on alkenone-based paleoceanographic indicators. Geochem., Geophys., Geosyst. 2 (29 January, 2000GC000122).

Grootes, P.M., Stuiver, M., 1997. Oxygen 18/16 variability in Greenland snow and ice with 10^{-3} to 10^{-5} year time resolution. J. Geophys. Res. 102 (C12), 26455–26470.

Gupta, A., Rahman, A., Poh Poh, W., Pitts, J., 1987. The old alluvium of Singapore and the extinct drainage system to the South China Sea. Earth Surf. Process. Landf. 12, 259–275.

Higginson, M.J., Maxwell, J.R., Altabet, M., in press. Nitrogen isotope and chlorin paleoproductivity records from the northern South China Sea: remote versus local forcing of millennial- and orbital-scale variability. Marine Geology.

Huang, C.-Y., et al., 1997. Deep sea and lake records of the Southeast Asian paleomonsoons for the last 25 thousands years. Earth Planet. Sci. Lett. 146, 59–72.

Ikehara, M., et al., 2000. Variations of terrestrial input and marine productivity in the Southern Ocean (48°S) during the last two deglaciations. Paleoceanography 15 (2), 170–180.

Jasper, J.P., Hayes, J.M., 1990. A carbon isotope record of CO_2 levels during the late quaternary. Nature 347, 462–464.

Jennerjahn, T.C., et al., 1992. Particle flux in the northern South China Sea. In: Jin, X.L., et al. (Eds.), Marine Geology and Geophysics of the South China Sea. China Ocean Press, Beijing, pp. 228–235.

Kienast, M., Steinke, S., Stattegger, K., Calvert, S.E., 2001. Synchronous tropical South China Sea sea surface temperature change and Greenland warming during deglaciation. Science 291, 2132–2134.

Kienast, M., Hanebuth, T.J.J., Pelejero, C., Steinke, S., 2003. Synchroneity of meltwater pulse 1a and the Bolling warming: new evidence from the South China Sea. Geology 31 (1), 67–70.

Koopmann, B., 1981. Saharan dust deposition in the subtropical Atlantic during the last 25,000 years (in German). Meteor-Forschungsergeb. C5, 23–54.

Lüdmann, T., Kin Wong, H., Wang, P., 2001. Plio-Quaternary sedimentation processes and neotectonics of the northern continental margin of the South China Sea. Mar. Geol. 172 (3–4), 331–358.

Middleburg, J.J., Soetaert, K., Herman, P.M.J., 1997. Empirical relationships for use in global diagenetic models. Deep-Sea Res., Part I 44 (2), 327–344.

Milliman, J.D., Meade, R.H., 1983. World-wide delivery of river sediment to the ocean. J. Geol. 1, 1–21.

Milliman, J.D., Farnsworth, K.L., Albertin, C.S., 1999. Flux and fate of fluvial sediments leaving large islands in the East Indies. J. Sea Res. 41 (1–2), 97–107.

Molengraaff, G.A.F., 1921. Modern deep-sea research in the East Indian Archipelago. Geogr. J. 57 (2), 95–121.

Ohkouchi, N., Kawamura, K., Kawahata, H., Taira, A., 1997a. Latitudinal distributions of terrestrial biomarkers in the sediments from the Central Pacific. Geochim. Cosmochim. Acta 61, 1911–1918.

Ohkouchi, N., Kawamura, K., Taira, A., 1997b. Fluctuations of terrestrial and marine biomarkers in the western tropical Pacific during the last 23,300 years. Paleoceanography 12 (4), 623–630.

Pagani, M., Freeman, K.H., Arthur, M.A., 1999. Late Miocene atmospheric CO_2 concentrations and the expansion of C_4 grasses. Science 285 (5429), 876–879.

Pelejero, C., Grimalt, J.O., 1997. The correlation between the U^{k}_{37} index and sea surface temperatures in the warm boundary: the South China Sea. Geochim. Cosmochim. Acta 61 (22), 4789–4797.

Pelejero, C., Grimalt, J.O., Heilig, S., Kienast, M., Wang, L., 1999a. High resolution U^{K}_{37}-temperature reconstructions in the South China Sea over the last 220 kyrs. Paleoceanography 14 (2), 224–231.

Pelejero, C., Kienast, M., Wang, L., Grimalt, J.O., 1999b. The flooding of Sundaland during the last deglaciation: imprints in hemipelagic sediments from the southern South China Sea. Earth Planet. Sci. Lett. 171, 661–671.

Peltzer, E.T., Gagosian, R.B., 1989. Organic geochemistry of aerosols over the Pacific Ocean. In: Riley, J.P., Chester, R. (Eds.), Chemical Oceanography, vol. 10. Academic Press, pp. 281–328.

Sarnthein, M., Wang, P., 1999. Response of West Pacific marginal seas to global climatic change. Mar. Geol. 156, 1–3.

Sarnthein, M., Pflaumann, U., Wang, P.X., Wong, H.K., 1994. Pre-

liminary report of the Sonne-95 cruise "Monitor Monsoon" to the South China Sea. Berichte—Reports, vol. 68. Geol.-Paläont. Inst. Univ., Kiel.

Schönfeld, J., Kudrass, H.R., 1993. Hemipelagic sediment accumulation rates in the South China sea related to late quaternary sea-level changes. Quat. Res. 40, 368–379.

Schubert, C.J., et al., 1998. Stable phytoplankton community in the Arabian Sea over the last 200,000 years. Nature 394, 563–566.

Shao, L., Li, X.H., Wei, G.J., Liu, Y., Fang, D.Y., 2001. Provenance of a prominent sediment drift on the northern slope of the South China Sea. Sci. China, Ser. D-Earth Sci. 44 (10), 919–925.

Stattegger, K., et al., 1997. Cruise report SONNE 115: Sundaflut—Sequence stratigraphy, late Pleistocene–Holocene sea level fluctuations and high resolution record of the post-Pleistocene transgression on the Sunda Shelf. Berichte—Reports, vol. 86. Geol.-Paläont. Inst. Univ., Kiel. 211 pp.

Steinke, S., Kienast, M., Hanebuth, T.J.J., in press. The importance of sea-level variations and shelf palaeo-morphology in governing shelf margin and slope sedimentation: examples from the southern South China Sea during the last deglaciation. Marine Geology.

Sun, X., Li, X., Beug, H.-J., 1999. Pollen distribution in hemipelagic surface sediments of the South China Sea and its relation to modern vegetation distribution. Mar. Geol. 156, 211–226.

Ternois, Y., Kawamura, K., Keigwin, L., Ohkouchi, N., Nakatsuka, T., 2001. A biomarker approach for assessing marine and terrigenous inputs to the sediments of Sea of Okhotsk for the last 27,000 years. Geochim. Cosmochim. Acta 65 (5), 791–802.

Thompson, S., Eglinton, G., 1978. The fractionation of a Recent sediment for organic geochemical analysis. Geochim. Cosmochim. Acta 42, 199–207.

Villanueva, J., Pelejero, C., Grimalt, J.O., 1997. Clean-up procedures for the unbiased estimation of C_{37}–C_{39} alkenone sea surface temperatures and terrigenous *n*-alkane inputs in paleoceanography. J. Chromatogr. 757, 145–151.

Villanueva, J., et al., 2001. A latitudinal productivity band in the Central North Atlantic over the last 270 kyr: an alkenone perspective. Paleoceanography 16 (6), 617–626.

Wang, P., 1999. Response of Western Pacific marginal seas to glacial cycles: paleoceanographic and sedimentological features. Mar. Geol. 156, 5–39.

Wang, L., Sarnthein, M., 1999. Long-/short-term variations of monsoon climate and its teleconnection to global change. In: Abrantes, F., Mix, A. (Eds.), Reconstructing Ocean History: A Window Into the Future. Kluwer Academic/Plenum Publishers, New York, pp. 57–71.

Wang, L., et al., 1999a. East Asian monsoon climate during the Late Pleistocene: high-resolution sediment records from the South China Sea. Mar. Geol. 156 (1–4), 243–282.

Wang, L., Sarnthein, M., Grootes, P., Erlenkeuser, H., 1999b. Millennial reoccurrence of century-scale abrupt events of East Asian monsoon: a possible heat conveyor for the global deglaciation. Paleoceanography, 725–731.